Tuning quantum dot properties by activated phase separation of an InGa(Al)As alloy grown on InAs stressors

M. V. Maximov, A. F. Tsatsul'nikov, B. V. Volovik, D. S. Sizov, Yu. M. Shernyakov, I. N. Kaiander, A. E. Zhukov, A. R. Kovsh, S. S. Mikhrin, V. M. Ustinov, and Zh. I. Alferov
A.F. Ioffe Physical-Technical Institute, Politekhnicheskaya 26, 194021, St. Petersburg, Russia

R. Heitz, V. A. Shchukin,* N. N. Ledentsov,* and D. Bimberg
Institut für Festkörperphysik, Technische Universität Berlin, D-10623 Berlin, Germany

Yu. G. Musikhin* and W. Neumann
Humboldt-Universität Berlin, Institut für Physik, Invalidenstrasse 110, D-10115 Berlin, Germany
(Received 18 May 2000; revised manuscript received 3 August 2000)

Strain-driven decomposition of an alloy layer is investigated as a means to control the structural and electronic properties of self-organized quantum dots. Coherent InAs/GaAs islands overgrown with an InGa(Al)As alloy layer serve as a model system. Cross-section and plan-view transmission electron microscopy as well as photoluminescence (PL) studies consistently indicate an increase in height and width of the island with increasing indium content and/or thickness of the alloy layer. The increasing island size is attributed to the phase separation of the alloy layer driven by the surface strain introduced by the initial InAs islands. The decomposition is enhanced by the addition of aluminum to the alloy layer. The ground-state transition energy in such quantum dots is significantly (up to 200 meV) redshifted compared to the original InAs/GaAs quantum dots, allowing to reach the 1.3 μm spectral region maintaining the high PL efficiency and the low defect density typical for Stranski-Krastanow growth. The possibility of degradation less stacking of such quantum dot layers enables injection lasing on the ground-state transition with a differential efficiency of 57% and a continuous-wave output power of 2.7 W.

I. INTRODUCTION

The formation of InAs/GaAs quantum dots (QD's) in highly lattice-mismatched epitaxy in the Stranski-Krastanow growth mode has attracted increasing interest in recent years. This growth mode provides an efficient means to fabricate dense arrays of virtually defect-free uniform QD's. Such self-organized QD's enabled us to take advantage of full three-dimensional confinement in optically[1] and then electrically[2] pumped laser devices, demonstrating the predicted superior temperature stability of the threshold current density.[2] Indeed, QD-based injection lasers are suitable candidates for the realization of low threshold current densities (J_{th}) and ultrahigh temperature stability at room temperature.[3–5] The self-organized growth provides, however, only limited control of the interrelated size and density of the islands, making it difficult to access the technologically important 1.3-μm region (for a recent review see, e.g., Ref. 6 and references therein). Extensive investigations have been conducted to overcome these limitations and to optimize the properties of QD arrays. Several approaches have been exploited to generate high-area densities of QD's providing sufficient localization for electrons and holes. In molecular beam epitaxy (MBE) the alternating deposition of group-III atoms and group-V molecules, e.g., by using alternating beams of In, As_2, Ga, and As_2,[7–9] as well as the use of a seed layer[10,11] have been successful. In metal organic chemical vapor deposition suitable large QD's can be realized by the deposition of $In_xGa_{1-x}As$ (Ref. 12) or by the periodic deposition of InAs and GaAs monolayers.[13]

The growth of large QD's is mostly based on exploiting the strain fields generated by nanoislands either free-standing or covered with a thin cap layer. For typical growth conditions, the bulk diffusion coefficients of atoms are several orders of magnitude smaller than surface ones, and thus bulk diffusion plays only a limited role during growth. Structural inhomogeneities, e.g., inclusions of a foreign material in a host matrix or composition modulations in an alloy, may arise due to the particularities of the surface kinetics at the advancing surface and persist after overgrowth. Such inhomogeneities create long-range strain fields, which direct the surface migration of adatoms. These strain fields are known to enhance phase separation in growing alloys, both lattice-matched[14–16] and lattice-mismatched[17,18] to the substrate. For example, the growth of multisheet arrays of QD's proceeds in such a way that formation of new islands is driven by the strain fields of the buried islands, resulting either in vertical correlation[19–22] or vertical anticorrelation[23] between the QD's of successive sheets depending on the spacer thickness.[24]

Here we report a detailed study of the surface-strain-driven phase separation of an InGa(Al)As alloy cap layer activated by predeposited InAs islands formed by Stranski-Krastanow growth.[25] The growth approach allows the controlled modification of the structural and optical properties of self-organized QD's, ultimately providing an effective means to fabricate uniform high-density QD ensembles for the 1.3-μm region, maintaining high optical quality.

II. SAMPLES AND EXPERIMENTAL SETUP

The investigated samples were grown by solid-source molecular beam epitaxy[26] (MBE) on GaAs(001) substrates us-

ing a Riber-32 MBE machine. GaAs and InAs were deposited at growth rates of 0.8 and 0.3 μm/h, respectively, and at an arsenic pressure of $(2-3)\times 10^{-6}$ Torr. After oxide desorption, an 0.5-μm-thick GaAs buffer was grown at 600 °C followed by a 2-nm/2-nm GaAs/AlAs short-period superlattice with six periods and a 100-nm GaAs spacer. Subsequently, the substrate temperature was lowered to 480 °C for the deposition of InAs, generating the InAs nanostressors. Different from conventional Stranski-Krastanow growth, these QD's are overgrown with an InGa(Al)As layer of variable composition and thickness. As will be shown below, this alloy layer undergoes strain-driven decomposition modifying the structural and optical properties of the InAs nanostressors. The first 10 nm of the subsequent GaAs cap layer were grown at the same temperature before the substrate temperature was increased back to 600 °C for the growth of 20 nm of GaAs, a 2-nm/2-nm GaAs/AlAs short-period superlattice with six periods, and a final 5-nm-thick GaAs layer for surface protection. The investigated laser structures were grown on Si-doped GaAs(001) substrate as described in detail in Ref. 27. These structures consist of a 0.4-μm-thick graded-index separate confinement heterostructure waveguide region confined by 1.5-μm-thick $Al_{0.4}Ga_{0.6}As$ cladding layers, which serve as *n*- and *p*-type emitters of nonequilibrium carriers. A 0.6-μm-thick GaAs p^+ contact layer was grown on top.

Transmission electron microscopy (TEM) measurements were performed in plan-view and cross-section geometry with a Phillips EM 420 microscope at an acceleration voltage of 100 kV. The average QD width was determined from a histogram of sizes estimated from plan-view TEM images for 100–200 dots. For photoluminescence (PL) measurements the samples were mounted in a closed-cycle He cryostat providing temperatures between 8 and 320 K. PL was excited by an Ar^+ laser with an excitation density of $\sim$200 W cm^{-2} if not stated otherwise. For PL excitation (PLE) experiments the samples were mounted in a continuous-flow He cryostat at 7 K. The light of a tungsten lamp dispersed by a 0.27-m double-grating monochromator served as tunable, low-excitation-density ($<$0.005 W cm^{-2}) light source. The luminescence was detected through a 0.5-m single-grating monochromator and a 0.3-m double-grating monochromator for PL and PLE measurements, respectively, using a cooled Ge diode.

III. EXPERIMENTAL RESULTS

In the present paper we study a new growth approach giving control of the structural and electronic properties of self-organized QD's, which we refer to as activated alloy phase separation (AAPS). A sheet of strained InAs islands is formed on the GaAs surface [Fig. 1(a)] by the deposition D_{IS} of 1.8–3.2 monolayer ML/InAs in the conventional Stranski-Krastanow mode and subsequently overgrown with an $Al_yIn_xGa_{1-x-y}As$ alloy layer [Figs. 1(b) and 1(c)]. The laterally varying surface strain caused by the InAs islands affects the overgrowth with an InGa(Al)As alloy layer by strain-driven surface migration. One may expect the following qualitative picture of the alloy phase separation activated by stressors. For the conventional overgrowth of InAs QD's by pure GaAs it has been found[28] that gallium atoms prefer

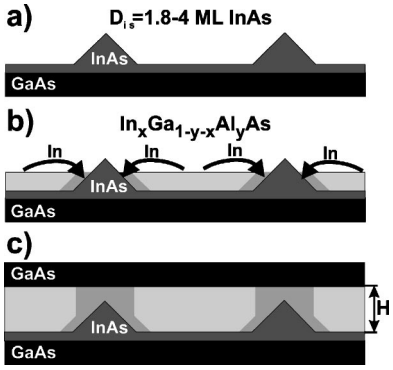

FIG. 1. Schematic diagram illustrating activated alloy phase separation. (a) Initial InAs stressors, (b) partial decomposition of the alloy layer due to strain-driven surface migration of indium, and (c) the final structure after GaAs capping.

to migrate away from the QD's towards pseudomorphically strained regions, having an in-plane local lattice constant equal to that of unstrained GaAs. A similar effect should occur during the overgrowth of InAs QD's by an InGa(Al)As alloy: Indium atoms will accumulate at the InAs QD's increasing their lateral size. When the QD's are completely covered the tensile strain on top of the QD's will favor indium accumulation from the growing alloy, probably increasing the effective height of the islands. Thus, we expect that AAPS increases the indium concentration in the vicinity of the islands on the expense of the indium concentration in the $In_xAl_yGa_{1-x-y}As$ alloy. In other words, AAPS potentially increases the width and height of the InAs islands providing for enhanced localization of electrons and holes. Figure 2 supports the expected trend showing plan-view TEM pictures of the original InAs islands covered by GaAs [panel (a)] as well as of such islands covered by a 5-nm $In_{0.15}Ga_{0.75}As$ layer [panels (b) and (c)]. Images (a) and (b) taken at $\mathbf{g}=220$ show a strong contribution of the local strain; image (c), taken under diffraction conditions far away from the exact Bragg orientation, allows for a more precise determination of the island size and shape. The TEM images show a clear increase of the width for islands capped with an $In_xGa_{1-x}As$ alloy. The estimated increase of the width from $\sim$12 to $\sim$18 nm supports the above-described qualitative model of AAPS. Below we will always quote QD widths and heights derived from TEM images taken under diffraction conditions far away from the exact Bragg orientation, similar to Fig. 2(c). Figure 3 shows cross-section TEM images for samples with 2.1 ML InAs initial islands capped either with (a) 5 nm of $In_{0.15}Ga_{0.85}As$ or (b) 5 nm of $In_{0.15}Al_{0.15}Ga_{0.7}As$. The effect of adding Al will be discussed in detail in Sec. III D. Note that the cross-sectional TEM images provide only a rough estimate for the height of the islands due to the uncertain In concentration profile generated in the AASP process. Detailed high-resolution electron microscopy (HREM), corresponding modeling, and cross-section scanning tunneling electron microscopy studies will be necessary to clarify the actual In profile.

From the above discussion it is clear that the AASP process will sensitively depend on the size and density of the InAs nanostressors, i.e., the initial InAs deposition amount, as well as on the thickness (H) and composition (x,y) of the $Al_yIn_xGa_{1-x-y}As$ alloy layer. Below we will describe in de-

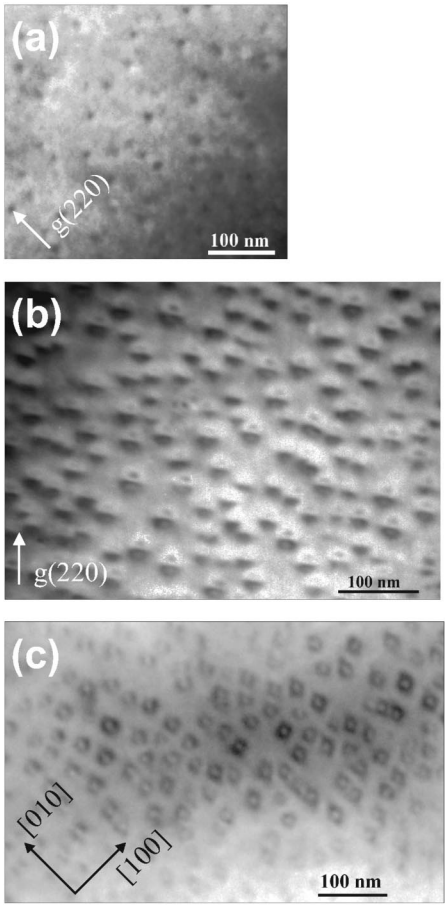

FIG. 2. Plan-view TEM images of (a) the initial Stranski-Krastanow islands and (b,c) QD's formed during the overgrowth with 5 nm of $In_{0.15}Ga_{0.85}As$. Images (a) and (b) were taken at $g = 220$, whereas image (c) was taken at diffraction conditions far away from exact Bragg orientation.

tail the dependence of the structural and photoluminescence properties of QD's formed by AAPS on the above-mentioned growth parameters.

A. Effect of the initial islands

The structural and optical properties of InAs/GaAs QD's formed in the Stranski-Krastanow growth mode have been extensively studied in recent years.[6,29–31] For the growth conditions applied in this work the continuous deposition of 4 ML of InAs on GaAs(001) at 480 °C and an arsenic pressure of 2×10^{-6} Torr leads to a dense array of equilibrium QD's, having a pyramidal shape with principal axes of the square base close to ⟨100⟩ and ⟨010⟩ directions.[32,33] The average pyramid base length is 12–14 nm and its height is 5–6 nm. A decrease of the InAs deposition to 2 ML produces much smaller and less uniform islands with pyramid base lengths of 8–9 nm. The change of the QD size is directly reflected in the ground-state transition energy, which at 10 K decreases monotonically from 1.26 to 1.09 eV [Fig. 4(a)] while the InAs deposition increases from 1.8 to 4 ML.[34] InAs depositions in excess of 4 ML lead to significant concentrations of plastically relaxed InAs islands due to the increased formation of extended defects (e.g., dislocation loops) and threading dislocations. Theoretical calculations of the electronic properties of such strained InAs pyramids with {101} side facets showed good agreement with the above-mentioned experimental data.[35] To first order, the QD ground-state transition energy can be taken as a measure for the island volume to relate structural and optical data. However, the exact shape as well as the indium concentration profile in and around the QD's will have to be taken into account for detailed predictions of the transition energies. The corresponding changes in the local strain distribution might have a pronounced effect on the electronic properties of the AASP QD's.

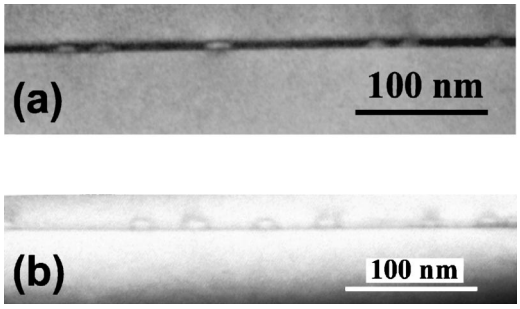

FIG. 3. Cross-sectional TEM images of samples with an initial InAs deposition $D_{IS} = 2.1$ ML overgrown either with 5-nm (a) $In_{0.15}Ga_{0.85}As$ or (b) $In_{0.15}Al_{0.15}Ga_{0.7}As$.

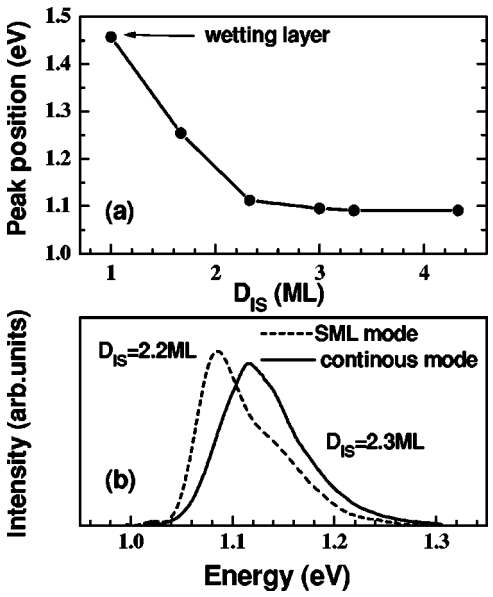

FIG. 4. (a) The ground-state transition energy of Stranski-Krastanow InAs/GaAs QD's vs the average InAs deposition amount D_{IS}, (b) PL spectra of InAs/GaAs QD islands formed by depositing 2.3 ML InAs in continuous mode and 2.2 ML InAs in submonolayer mode ($T = 10$ K).

One way to increase the size of the initial InAs islands for a given deposition amount is to reduce the growth rate applying a submonolayer (SML) growth mode or alternating beams of In, Ga, and As_2.[7–9] Figure 4(b) compares PL spectra of InAs/GaAs islands for 2.2 ML InAs SML deposition and 2.3 ML InAs continuous deposition. Obviously the SML growth mode generates larger islands than the conventional continuous one. Furthermore, the QD size can be affected by a growth interruption following the InAs deposition. For instance, for our growth conditions a 100-sec growth interrup-

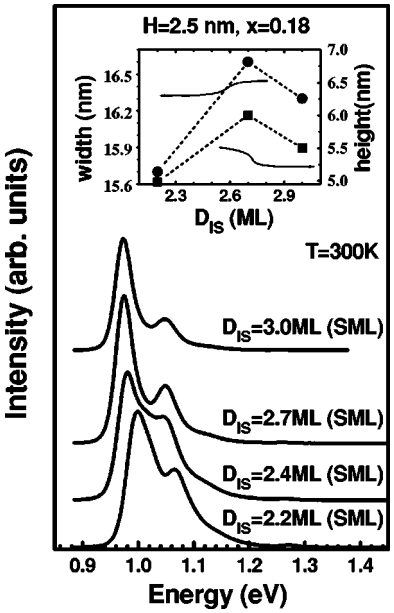

FIG. 5. PL spectra of AAPS QD's for various InAs deposition amounts D_{IS} (SML mode) for constant thickness ($H=2.5$ nm) and composition ($x=0.18$) of the $In_xGa_{1-x}As$ alloy. The inset shows the width and height of the QD's determined from TEM images.

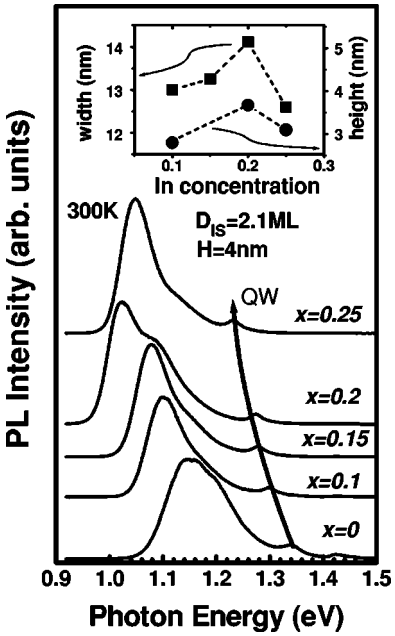

FIG. 6. PL spectra of AAPS QD's for various In concentrations x of the alloy for a constant InAs deposition amount ($D_{\mathrm{IS}}=2.1$ ML) and thickness ($H=4$ nm) of the $In_xGa_{1-x}As$ alloy. The inset shows the width and height of the QD's determined from TEM images.

tion after the deposition of 2 ML InAs increases the QD size from 7–9 to 12–14 nm with a corresponding ~170-meV redshift of PL line.[32] It was, however, impossible to shift the PL maximum further beyond 1.4 μm at 10 K using conventional InAs/GaAs QD's.

Figure 5 shows the effect of the amount D_{IS} of InAs deposited in the SML mode on the PL spectra of samples overgrown with 2.5-nm $In_{0.18}Ga_{0.82}As$. The QD PL shifts to lower energies with increasing D_{IS}. The inset shows the concomitant variation of QD size and height obtained from TEM studies to be in qualitative agreement with the PL data. The width (height) of the QD's increases from 15.7 (4.9) to 16.6 nm (6.0 nm) increasing D_{IS} from 2.2 to 2.7 ML. When D_{IS} exceeds 2.7 ML the redshift saturates and the PL intensity starts to decrease. TEM images suggest a sudden increase of the dislocation density above a critical deposition of ~2.7 ML, providing an efficient means for local strain relaxation. The dislocation density was estimated to $1\times10^8\,\mathrm{cm}^{-2}$ for 2.7 ML InAs deposition. Such dislocations have a significant effect on the island evolution on the surface since they attract InAs from both the alloy and already formed QD's. Ultimately, the QD size and height saturate or may even decrease again. Simultaneously, the redshift of PL line saturates at 2.7 ML and the PL intensity drops. For $D_{\mathrm{IS}}=3.0$ MLInAs the dislocation density increases to $3\times10^8\,\mathrm{cm}^{-2}$. Note that the initially elastically strained InAs islands become dislocated only during overgrowth. The total strain energy increases due to the additional InAs accumulation at the islands, favoring dislocation formation.

Figure 5 suggests an optimum InAs deposition amount for achieving efficient long-wavelength emission maintaining the low dislocation density. The optimum will, however, depend also on the composition (x) and thickness (H) of the alloy layer.

B. Effect of alloy composition and thickness

Figure 6 compares PL spectra of samples for which the initially deposited 2.1 ML InAs (continuous deposition) have been overgrown with a 4-nm-thick $In_xGa_{1-x}As$ alloy layer with indium compositions x between 0 and 0.25. The initial islands ($x=0$) show PL at 1.14 eV with a full width at half maximum (FWHM) of 100 meV. With increasing indium content x the PL peak shifts to lower energies and becomes narrower. The weak emission line appearing ~200 meV above the QD ground-state transition is attributed to the quantum well (QW) formed by the InAs wetting layer covered by the residual $In_xGa_{1-x}As$ alloy layer. The identification of the QW peak is confirmed by PLE studies, as will be shown below. The thickness of the QW layer is constant (4 nm), and thus the redshift of the QW emission peak with increasing indium composition is attributed to the decreasing band gap of the alloy layer.

Interestingly, the QD and QW PL peaks behave differently with increasing indium content, also suggesting structural changes. For indium concentrations x in excess of 0.2 the QW emission is still redshifted, reflecting the increased In content of the residual alloy layer, whereas the QD emission is again blueshifted. The insert shows the QD width and height obtained from TEM images via the indium content. The QD width (height) increases from 13.2 (2.8) nm to 14.1 (3.7) nm increasing the indium content from 0.1 to 0.2, and subsequently decreases to 12.6 (3.1) nm for $x=0.25$ in qualitative agreement with the evolution of the QD transition energy. The changing QD volume correlates to a changing localization of the exciton wave function and transition energy. The decrease of the QD width and height (as well as the corresponding blueshift) observed for $x>0.2$ is attributed to

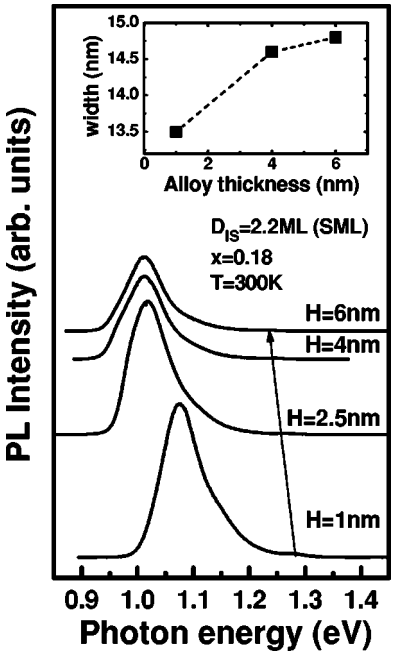

FIG. 7. PL spectra of AAPS QD's for various thicknesses H of the alloy for a constant InAs deposition amount ($D_{\mathrm{IS}}=2.1$ ML, SML mode) and composition ($x=0.18$) of the $In_xGa_{1-x}As$ alloy. The inset shows the width of the QD's determined from TEM images.

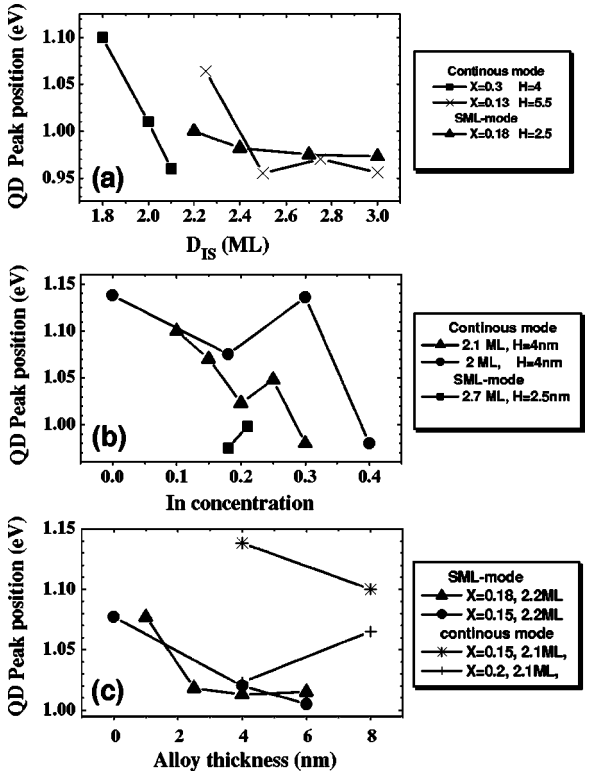

FIG. 8. Dependence of the ground-state transition energy ($T=300$ K) of AAPS QD's on (a) the InAs deposition amount D_{IS} as well as (b) the In content x and (c) thickness H of the $In_xGa_{1-x}As$ alloy layer.

the increased formation of dislocations that absorb indium from the alloy and maybe also from already formed AAPS QD's.

The effect of the thickness of the $In_xGa_{1-x}As$ alloy layer on the AAPS-formed QD's is shown in Fig. 7 for an indium composition $x=0.18$ and a SML InAs deposition of 2.2 ML. The increase of the thickness of the $In_xGa_{1-x}As$ alloy layer from 1 to 2.5 nm leads to an ~100-meV redshift of the ground-state transition. Further increasing the thickness results only in a decrease in the PL intensity for practically constant transition energy. The initial low-energy shift for small alloy thickness is connected to an increase of the island width (inset). The increase in QD width and corresponding redshift of the PL line saturates at a certain critical thickness. Further increasing the thicknesses leads only to a decrease of the PL yield, suggesting enhanced dislocation formation. Again, this effect is attributed to the total strain energy exceeding a critical value for dislocation formation.

C. Optimization of growth parameters

Figures 5–7 suggest that the three-parameter space given by D_{IS}, x, and H enables us to generate QD's with highly efficient long-wavelength emission. However, due to the intricacies of the AAPS process all three parameters are interrelated, Fig. 8. Panel (a) summarizes the dependence of QD transition energy (E_{PL}) on D_{IS}. For $x=0.13$ and $H=5.5$ nm the dependence of E_{PL} on D_{IS} is qualitatively similar to that presented in Fig. 5. An increase of D_{IS} from 2.25 to 2.5 ML results in a very strong 100-meV redshift of the PL line, approaching 1.3 μm at 300 K. A further increase in D_{IS} to 3.0 ML leads only to a decrease of the PL intensity due to formation of dislocations. For $x=0.3$ and $H=4$ nm the strong (>100-meV) redshift of the PL line occurs already when D_{IS} increases from 1.8 to 2.0 ML. For such a high indium content dislocation formation is already enhanced for $D_{\mathrm{IS}}=2.0$ ML ($\rho_{\mathrm{dis}}=1.4\times10^9$) limiting the potential of such samples for practical applications.

Figure 8(b) shows the effect of the indium concentration on the ground-state transition energy E_{PL} for an alloy thickness of 4 nm and indium depositions D_{IS} of 2.0 and 2.1 ML (SML mode). Both data show an intermediate blueshift for $0.2<x<0.3$, i.e., for indium contents higher than the critical one for enhanced dislocation formation. Very high indium compositions ($x>0.3$) allow reaching of the 1.3-μm wavelength region. The high dislocation density [$\rho_{\mathrm{dis}}=(3-9)\times10^9$] of such samples leads, however, to a dramatic (>100 times) decrease of the PL yield. Interestingly, a small increase in D_{IS} leads to a significant redshift of PL transition for large x in agreement with the results presented in Fig. 8(a).

The effect of the alloy thickness H on the ground-state transition energy E_{PL} depends drastically on the indium content x [panel (c)]. For large indium concentrations ($x=0.18$ and $x=0.2$) the saturation of the redshift or even blueshift begins already at $H=4$ nm [see also Fig. 8(b)], whereas for $x=0.15$ it is not observed up to 6 nm ($D_{\mathrm{IS}}=2.2$ ML, SML mode) or 8 nm ($D_{\mathrm{IS}}=2.1$ ML, continuous mode).

The PL and TEM data presented in Figs. 5–8 suggest a narrow range of *interrelated* values for the InAs deposition (D_{IS}) as well as the $In_xGa_{1-x}As$ alloy thickness (H) and composition (x) allowing to achieve emission in the 1.3-μm spectral region maintaining a high PL efficiency and low

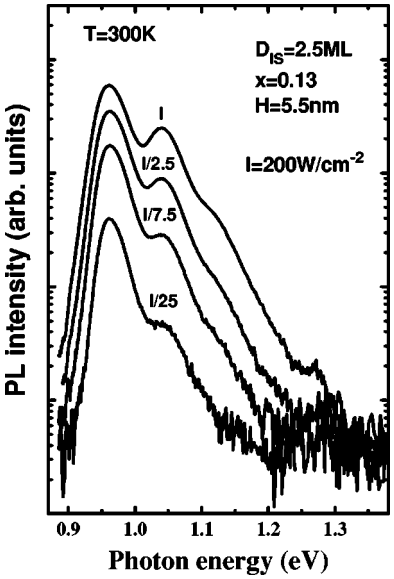

FIG. 9. PL spectra of AAPS QD's ($D_{IS}=2.5$ ML, $x=0.13$, $H=5.5$ nm) for various excitation densities.

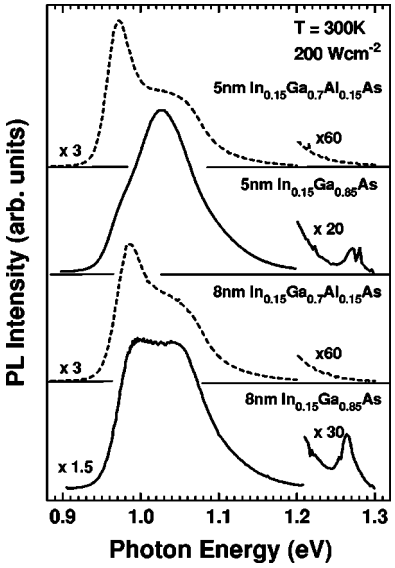

FIG. 10. PL spectra for AAPS QD's formed by activated alloy phase separation of an $In_{0.15}Ga_{0.85}As$ (solid curves) and $In_{0.15}Al_{0.15}Ga_{0.7}As$ (dashed-dot curves) alloy layer. For all samples, the nanostressors were formed by the deposition of 2.1 ML InAs in the SML mode.

dislocation density. For the growth conditions used the optimal parameters are $D_{IS}=2.5-2.7$ ML, $x=12-15\,\%$, and $H=4-6$ nm.

Figure 9 shows PL spectra of a sample emitting near 1.3 μm as a function of the excitation density. At the lowest excitation density the emission mainly originates from the ground-state transition with a energy shoulder resolved only in a logarithmic scale. With increasing excitation density the ground-state transition starts to saturate and subsequently the first and second excited-state transitions gain intensity. Emission from quantum well leads to a weak peak at 1.27 eV. Each of the high-energy QD peaks is likely to be a superposition of two or more closely located peaks from transitions involving different electron and hole sublevels.[11] A conclusive discussion of the electronic properties of the AAPS QD's will, however, depend on detailed numerical calculations.[35] In addition to the altered structural properties of the initial InAs islands studied here, also the altered redistribution[36,37] and the partial lowering of the barrier band gap[38–40] due to the $In_xGa_{1-x}As$ alloy layer will play a role.

D. Effect of aluminum

Further experimental insights into the effect of the altered structural properties of the AAPS QD's on the electronic properties can be obtained adding aluminum to the alloy layer, changing the chemical composition (and the band gap) of the alloy layer for a constant lattice mismatch. Aluminum is known to enhance the effect of phase separation in strained $In_xAl_yGa_{1-x-y}As$ quantum wells.[41] Figure 10 shows the effect of adding 15% aluminum to the $In_{0.15}Ga_{0.85}As$ alloy on the PL spectra. Initially 2.2 ML InAs were deposited in SML mode and overgrown with alloys of thickness $H=5$ and 8 nm. Although the $In_{0.15}Al_{0.15}Ga_{0.7}As$ band gap is about 150 meV larger than that of $In_{0.15}Ga_{0.85}As$, increasing the barrier potential, the QD ground-state transition energy decreases by $\sim$60 meV for $H=5$ nm. This redshift is a clear fingerprint of an increase of the volume of the AAPS islands and therefore altered surface kinetics in the presence of aluminum. Replacing gallium with aluminum does not alter the strain distribution and the increased barrier height should cause a blueshift. Cross-sectional TEM images of the samples with a 5-nm $In_{0.15}Ga_{0.85}As$ and $In_{0.15}Al_{0.15}Ga_{0.7}As$ alloy layer are compared in Figs. 3(a) and 3(b), respectively. AAPS QD's formed from the $In_{0.15}Ga_{0.85}As$ alloy have a width of 18 nm and a height of 4–5 nm. Adding aluminum increases the width slightly to 18.5 nm and the height considerably to 5.5–6.5 nm. The increasing QD height supports an enhancement of AAPS effects in the $Al_yIn_xGa_{1-x}As$ alloy layer. The situation is more complex in case of a thicker alloy layer ($H=8$ nm). Here, the increased strain energy enhances dislocation formation, accumulating indium. Correspondingly, the PL energy remains unaltered or even blueshifts, adding aluminum or increasing the alloy thickness (Fig. 10).

The overgrowth of InAs Stranski-Krastanow islands with pure AlAs leads to a redistribution of indium on the surface.[42,43] Aluminum atoms substitute indium atoms in the wetting layer, which then accumulate at the three-dimensional (3D) islands, increasing the island volume. A possible explanation might be that the total surface energy of an ultrathin AlAs(100) layer is smaller than that of the InAs wetting layer at the growth temperature. The redistribution of indium atoms predominantly increases the island height and may be considered as transition from a Stranski-Krastanow to a Volmer-Weber-like island arrangement. The present results (Figs. 3 and 10) suggest that the relatively small ($x=0.15$) aluminum content is sufficient to drive the redistribution of indium atoms increasing the island height.

Adding aluminum to the alloy layer should dramatically alter the properties of the QW composed of the InAs wetting layer and the alloy layer. A pronounced blueshift of the QW transition is expected, and effective-mass calculations indicate the possibility of suppressing any bound states in the QW structure. Indeed, the PL spectra shown in Fig. 10 show

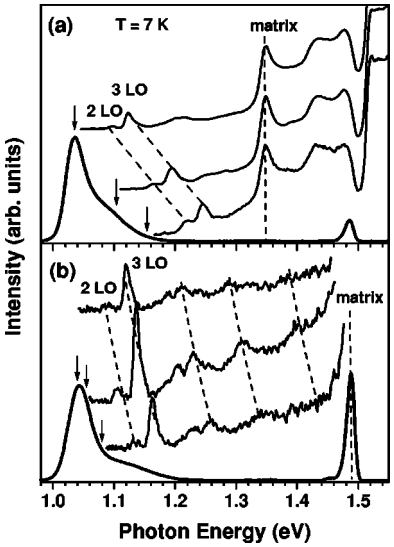

FIG. 11. PL and PLE spectra of AAPS QD's formed by activated alloy phase separation of an (a) $In_xGa_{1-x}As$ and (b) $In_xAl_yGa_{1-x-y}As$ alloy layer. The detection energies of the PLE spectra are indicated by arrows.

a weak resonance at ~1.27 eV for samples with an $In_xGa_{1-x}As$ alloy layer, which is missing aluminum to the alloy in agreement with the behavior expected of the QW. Photoluminescence excitation (PLE) measurements on different samples, Fig. 11, support this interpretation. Starting from the detection energy a series of almost equidistant PLE resonances evolves with increasing excitation energy. The energy spacing between the resonances of ~32 meV is close to the InAs QD LO-phonon energy.[44] For the sample with an $In_{0.15}Ga_{0.85}As$ alloy layer [panel (a)] a strong resonance is observed at 1.35 eV, independent of the detection energy. The transition is attributed to the QW formed by the combined wetting layer and alloy layer. For the sample with an $In_xGa_{1-x-y}Al_yAs$ alloy layer [panel (b)] no QW transition is revealed in the PLE spectra up to 1.48 eV. Thus, adding aluminum to the alloy results in QD's providing exceptionally high localization exceeding 400 meV with respect to both the 2D and 3D continuum states.

E. Stacking of AAPS QD's

An important aspect of QD formation is the potential to achieve three-dimensional packing. For example, the saturated modal gain of a single QD dense layer of only a few inverse centimeters is not sufficient to achieve lasing in short-cavity devices. For conventional Stranski-Krastanow growth it is necessary to apply small spacers in order to maintain or improve the optical properties.[19,45] However, small (Al, Ga)As spacers provide for strong electronic coupling and each stack of QD's can be considered as a single quantum-mechanical object.[20] In order to achieve the inherent benefits from three-dimensional packaging it is necessary to increase the spacer thickness to some 10 nm, avoiding electronic coupling of the QD's.[46]

In contrast, stacking of AAPS QD's allows the use of thick spacer layers without degradation of the optical properties; see Fig. 12. Panel (a) shows the effect of a rather thin spacer of ~5 nm. The ground-state transition experiences a

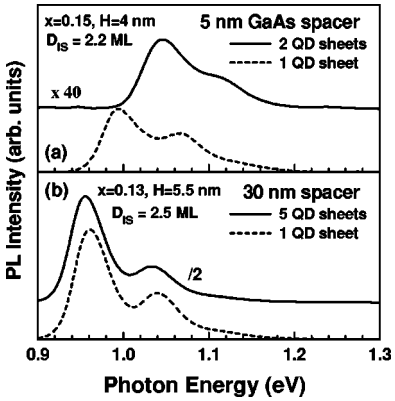

FIG. 12. PL spectra of single-layer and multiply stacked AAPS QD structures. The thicknesses of the GaAs spacer separating the QD layers are (a) 5 nm and (b) 30 nm.

50-meV blueshift accompanied by a 40-times decrease in PL yield in the stacked sample. In contrast, applying thick (>30 nm) GaAs spacers maintains the emission wavelength and the high PL efficiency under the used growth conditions [Fig. 12(b)]. The altered strain distribution around the AAPS QD's provides for a smaller amplitude of the lateral modulation of the surface stress and, therefore, for less strain interaction in the multilayered samples. Furthermore, the stacking of QD's is limited by the formation of large dislocated clusters. Even small densities of such clusters in the first QD sheet can result in a dramatic deterioration of the structural and optical properties of subsequent sheets in multilayered QD structures.[47] The formation of such large clusters might, however, be suppressed by a special annealing technique.[47] The annealing step was performed as follows: the QD's were overgrown with a thin GaAs layer (2 nm) at 480 °C and then the substrate temperature was raised to 600 °C. The thin cap layer only partly covers the large dislocated InAs clusters, allowing the InAs to evaporate in the annealing step. The smaller coherent QD's, being completely covered, are only weakly affected. According to deep level transient spectroscopy (DLTS) studies of the structures subjected to this procedure, $EL2$ and $EL3$ traps, associated with dislocations are completely suppressed in the DLTS spectra, and the concentration of deep traps associated with point defects is reduced by more than an order of magnitude.[48] Panel (b) compares PL spectra for a single- and fivefold QD structure. The latter was grown with the annealing step and a spacer thickness of 30 nm. The thick spacer prevents the degradation of the PL intensity, the blueshift, and/or the broadening of the PL line. Laser studies (see below) confirm the high structural and optical quality of such multilayered QD structures.

IV. ELECTROLUMINESCENCE AND LASING IN QD's FORMED BY AAPS

InAs QD's grown on GaAs substrates are very promising candidates to replace the traditional InP-based long-wavelength QW devices.[27,38–40,49–53] The performance of state-of-the-art InP-based QW devices is limited by a strong temperature sensitivity of their characteristics caused by insufficient electron confinement in the active region.[54,55] In contrast, InAs/GaAs QD's providing much stronger carrier localization might potentially improve the poor temperature

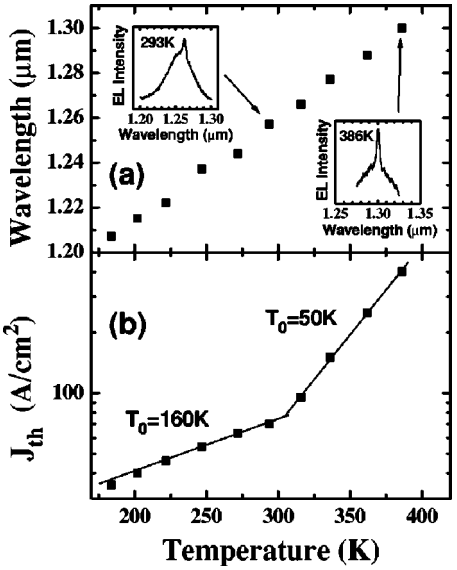

FIG. 13. (a) Emission wavelength and (b) threshold current density for lasers based on three-fold stacked AAPS QD's (four-side cleaved-edge geometry). Lasing spectra at 293 and 384 K are shown in the insets of panel (a).

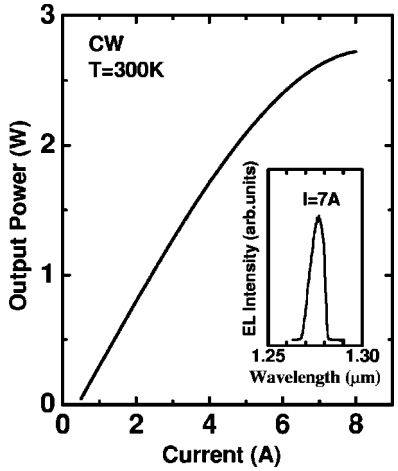

FIG. 14. True continuous-wave light-current characteristics of a laser based on three-fold stacked AAPS QD's at $T=300$ K. The inset shows a lasing spectrum at 7 A.

characteristics of the present 1.3- and 1.55-μm emitting lasers. Moreover, the InAs-GaAs-AlAs material system allows for the fabrication of monolithic high-contrast lattice-matched GaAs-AlAs distributed Bragg reflectors for vertical-cavity surface-emitting lasers (VCSEL's) and cavity-enhanced photodetectors. The need to increase the size of such InAs/GaAs QD's to reach the technologically important spectral regions generally caused enhanced formation of defects and dislocated clusters, which severely affect the electrical and optical properties. The large dislocated clusters, comprising the smallest band-gap regions, are sources of nonradiative leakage currents. However as shown above, the AAPS growth approach allows us to reach the 1.3 μm region avoiding enhanced defect and dislocation formation. The AAPS QD's are thus ideally suited for the realization of high-performance GaAs-based 1.3-μm injection lasers.

Figure 13(a) shows the threshold current density and emission wavelength for an injection laser based on threefold stacked AAPS QD's as a function of temperature. The device was fabricated with four cleaved edges to minimize mirror losses. The insets depict lasing spectra at 293 and 384 K, revealing lasing at 1.28 and 1.30 μm, respectively. In the investigated temperature range the lasing wavelength is close to the ground-state transition energy observed in PL spectra at low excitation densities. Obviously lasing occurs via the QD ground-state transition. Panel (b) depicts the temperature evolution of the threshold current density. The threshold current density and the characteristic temperature T_0 at room temperature are, respectively, 80 A cm^{-2} and 160 K. Figure 14 shows the light-current characteristics and lasing spectra for a 1.9-mm-long shallow-mesa stripe laser obtained in under true continuous-wave operation. The differential efficiency is ~57% and a maximum output power of 2.7 W limited by thermal rollover is achieved.

In Refs. 51 and 52 the spontaneous emission characteristics of 1.3-μm-emitting QD's grown using alternating beams of In, As_2, Ga, and As_2 were studied as a function of the current density and temperature. A strong increase of nonradiative recombination was observed with increasing current density and temperature. This effect may be attributed to an increased concentration of nonradiative recombination centers in QD structures. Such nonradiative leakage would explain the low differential efficiency (~2%) and the switching from ground- to excited-state lasing at 1.18 times the threshold current (J_{th}) in corresponding laser devices.

In contrast, the improved material quality achieved with the AAPS growth approach yields differential efficiencies as high as 57% at 15 °C, which decreases only slightly to 53%, raising the temperature to 60 °C (Fig. 15). Ground-state lasing is observed up to (at least) 90 °C (Fig. 13) and up to driving currents as high as $16\times J_{th}$ (Fig. 14). These results support the high optical and structural quality of QDs formed by AAPS and demonstrate their potential for 1.3 μm edge-emitting lasers for telecommunications.

High-performance long-wavelength QD laser have also been realized by the dots-in-the-well (DWELL) growth technique,[38–40] which seems to be similar to AAPS. In the

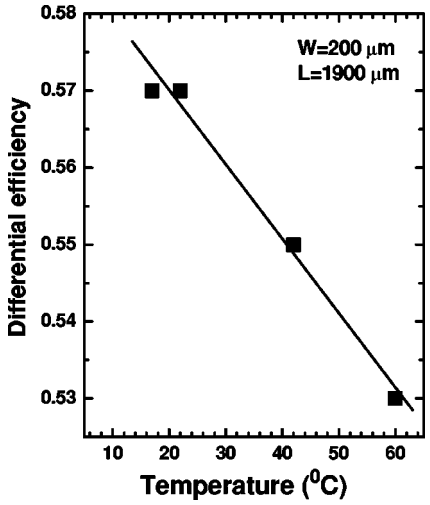

FIG. 15. Temperature dependence of the differential efficiency of a laser based on three-fold stacked AAPS QD's. The stripe length and thickness were 1900 and 200 μm, respectively.

DWELL growth approach the initial islands ($D_{IS}=2.4$ ML InAs) were formed on a 5-nm-thick $In_xGa_{1-x}As$ ($x=0.15,0.20$) buffer and then overgrown with a 5-nm-thick $In_xGa_{1-x}As$ alloy. The emission wavelength was 1.26 μm with a threshold current density of 26 A cm^{-2} and a differential efficiency of 31%.[38–40]

Very recently pulsed lasing at 1.3 μm has been demonstrated for vertical-cavity surface emitting lasers with the active region based on three sheets of QD's formed by AAPS. The threshold current was 1.8 mA for an 8×8-μm^2 oxidized aperture. A differential efficiency of 45% (20 °C) was achieved.[56]

V. CONCLUSIONS

To conclude, we have studied QD's formed by activated phase separation of an InGa(Al)As alloy layer grown on InAs nanostressors. Strain-driven surface kinetics was shown to lead to a partial decomposition of the alloy layer increasing the size of the initial InAs nanostressors. This growth approach allows achieving highly efficient emission at 1.3 μm and exciton localization energies in excess of 400 meV for GaAs-based structures. The high material quality achieved with the AAPS growth technique permits ground-state transition lasing up to 90 °C and up to driving currents as high as $16J_{th}$ (at room temperature).

ACKNOWLEDEGMENTS

Parts of this work are supported by Volkswagen Stiftung, BMBF, INTAS, and the Russian Foundation for Basic Research. M.V.M. and V.A.Sh. are thankful to the Alexander von Humboldt Foundation. N.N.L. is a DAAD professor. Yu.G.M. acknowledges support from INTAS (reference No. YSF99-204).

*On leave from A.F. Ioffe Institute.

[1] N. N. Ledentsov, V. M. Ustinov, A. Yu. Egorov, A. E. Zhukov, M. V. Maximov, I. G. Tabatadze, and P. S. Kop'ev, Fiz. Tekh. Poluprovodn. [Semiconductors **28**, 832 (1994)].

[2] N. Kirstaedter, N. N. Ledentsov, M. Grundmann, D. Bimberg, V. M. Ustinov, S. S. Ruvimov, M. V. Maxirnov, P. S. Kop'ev, Zh. I. Alferov, U. Richter, P. Werner, U. Gosele, and J. Heydenreich, Electron. Lett. **30**, 1416 (1994).

[3] L. V. Asryan and R. A. Suris, Semicond. Sci. Technol. **11**, 554 (1996).

[4] M. Grundmann and D. Bimberg, Jpn. J. Appl. Phys., Part 1 **36**, 4181 (1997).

[5] L. V. Asryan and R. A. Suris, IEEE J. Quantum Electron. **34**, 841 (1998).

[6] D. Bimberg, M. Grundmann, and N. N. Ledentsov, *Quantum Dot Heterostructures* (Wiley, Chichester, 1999).

[7] G. E. Tsyrlin, A. O. Golubok, S. Ya. Tipisev, and N. N. Ledentsov, Fiz. Tekh. Poluprovodn. **29**, 1697 (1995) [Semiconductors **29**, 884 (1995)].

[8] G. M. Guryanov, G. E. Cirlin, V. N. Petrov, N. K. Polyakov, A. O. Golubok, S. Ya. Tipissev, E. P. Misikhina, V. B. Gubanov, Yu. B. Samsonenko, and N. N. Ledentsov, Surf. Sci. **331-333**, 414 (1995).

[9] R. P. Mirin, J. P. Ibbetson, K. Nishi, A. C. Gossard, and J. E. Bowers, Appl. Phys. Lett. **67**, 3795 (1995).

[10] I. Mukhametzhanov, R. Heitz, J. Zeng, P. Chen, and A. Madhukar, Appl. Phys. Lett. **73**, 1341 (1998).

[11] R. Heitz, I. Mukhametzanov, A. Madhukar, A. Hoffmann, and D. Bimberg, J. Electron. Mater. **28**, 520 (1999).

[12] F. Heinrichsdorff, M. Grundmann, O. Stier, A. Krost, and D. Bimberg, J. Cryst. Growth **195**, 540 (1998).

[13] K. Mukai, O. Nobuyuki, S. Mitsuru, and S. Yamzaki, Jpn. J. Appl. Phys., Part 2 **33**, L1710 (1994).

[14] V. G. Malyshkin and V. A. Shchukin, Fiz. Tekh. Poluprovodn. [Semiconductors **27**, 1062 (1993)].

[15] I. P. Ipatova, V. G. Malyshkin, A. A. Maradudin, V. A. Shchukin, and R. F. Wallis, in *Proceedings of the 23rd International Symposium on Compound Semiconductors, St. Petersburg, Russia, September 1996*, Inst. Phys. Conf. Ser. No. 155, 323 (IOP, Bristol, 1997), p. 323; Phys. Rev. B **57**, 12 968 (1998).

[16] V. A. Shchukin and A. N. Starodubtsev, in Proceedings of the 26th International Symposium on Compound Semiconductors, Berlin, Germany (IOP, Bristol, 2000), p. 231.

[17] J. E. Guyer and P. W. Voorhees, Phys. Rev. Lett. **74**, 4031 (1995); Phys. Rev. B **54**, 11 710 (1996).

[18] F. Léonard and R. C. Desai, Phys. Rev. B **57**, 4805 (1998).

[19] Q. Xie, A. Madhukar, P. Chen, and N. P. Kobayashi, Phys. Rev. Lett. **75**, 2542 (1995).

[20] N. N. Ledentsov, V. A. Shchukin, M. Grundmann, N. Kristaedter, J. Böhrer, O. Schmidt, D. Bimberg, S. V. Zaitsev, V. M. Ustinov, A. E. Zhukov, P. S. Kop'ev, Zh. I. Alferov, A. I. Borovkov, A. O. Kosogov, S. S. Ruvimov, P. Werner, U. Gösele, and J. Heydenreich, Phys. Rev. B **54**, 8743 (1996).

[21] M. V. Maximov, D. A. Bedarev, A. Yu. Egorov, P. S. Kop'ev, A. R. Kovsh, A. V. Lunev, Yu. G. Musikhin, Yu. M. Shernyakov, A. F. Tsatsul'nikov, V. M. Ustinov, B. V. Volovik, A. E. Zhukov, Zh. I. Alferov, N. N. Ledentsov, and D. Bimberg, in *Proceedings of the 24th International Conference of Physics, Jerusalem, August 1998*, edited by D. Gershoni (World Scientific, Singapore, 1999).

[22] R. Heitz, A. Kalburge, Q. Xie, M. Grundmann, P. Chen, A. Hoffmann, A. Madhukar, and D. Bimberg, Phys. Rev. B **57**, 9050 (1998).

[23] I. L. Krestnikov, M. Straßburg, M. Caesar, A. Hoffmann, U. W. Pohl, D. Bimberg, N. N. Ledentsov, P. S. Kop'ev, Zh. I. Alferov, D. Litvinov, A. Rosenauer, and D. Gerthsen, Phys. Rev. B **60**, 8695 (1999).

[24] V. A. Shchukin, D. Bimberg, V. G. Malyshkin, and N. N. Ledentsov, Phys. Rev. B **57**, 12 262 (1998).

[25] B. V. Volovik, A. F. Tsatsul'nikov, D. A. Bedarev, A. Yu. Egorov, A. E. Zhukov, A. R. Kovsh, N. N. Ledentsov, M. V. Maksirnov, N. A. Maleev, Yu. G. Musikhin, A. A. Suvorova, V. M. Ustinov, P. S. Kop'ev, and Zh. I. Alferov, Fiz. Tekh. Poluprovodn. [Semiconductors **33**, 901 (1999)].

[26] N. N. Ledentsov, *Growth Processes and Surface Phase Equilibria in Molecular Beam Epitaxy*, Springer Tracts in Modern Physics (Springer, Berlin, 1999), Vol. 156.

[27] A. E. Zhukov, V. M. Ustinov, A. R. Kovsh, A. Yu. Egorov, N. A. Maleev, N. N. Ledentsov, A. F. Tsatsul'nikov, M. V. Maximov, Yu. G. Musikhin, N. A. Bert, P. S. Kop'ev, D. Bimberg, and Zh. I. Alferov, Semicond. Sci. Technol. **14**, 575 (1999).

[28] Q. Xie, P. Chen, and A. Madhukar, Appl. Phys. Lett. **65**, 2051 (1994).
[29] L. Goldstein, F. Glas, J. Y. Marzin, M. N. Charasse, and G. Le Roux, Appl. Phys. Lett. **47**, 1099 (1985).
[30] S. Guha, A. Madhukar, and K. C. Rajkumar, Appl. Phys. Lett. **57**, 2110 (1990).
[31] J. M. Moison, F. Houzay, F. Barthe, L. Leprice, E. Andre, and O. Vatel, Appl. Phys. Lett. **64**, 196 (1994).
[32] N. N. Ledentsov, M. Grundmann, N. Kirstaedter, O. Schmidt, R. Heitz, J. Böhrer, D. Bimberg, V. M. Ustinov, V. A. Shchukin, P. S. Kop'ev, Zh. I. Alferov, A. O. Kosogov, P. Werner, U. Richter, U. Gösele, and J. Heydenreich, Solid-State Electron. **40**, 785 (1996).
[33] M. Grundmann, N. N. Ledentsov, R. Heitz, L. Eckey, J. Christen, J. Böhrer, D. Bimberg, S. S. Ruvimov, P. Werner, U. Richter, J. Heydenreich, V. M. Ustinov, A. Yu. Egorov, A. E. Zhukov, P. S. Kop'ev, and Zh. I. Alferov, Phys. Status Solidi B **188**, 249 (1995).
[34] A. Yu. Egorov, A. E. Zhukov, P. S. Kop'ev, N. N. Ledentsov, M. V. Maximov, V. M. Ustinov, A. F. Tsatsul'nikov, and Zh. I. Alferov, Fiz. Tekh. Poluprovodn. **30**, 707 (1996) [Semiconductors **30**, 707 (1996)].
[35] O. Stier, M. Grundmann, and D. Bimberg, Phys. Rev. B **59**, 5688 (1999).
[36] K. Nishi, H. Saito, S. Sugou, and J.-S. Lee, Appl. Phys. Lett. **74**, 1111 (1999).
[37] N.-T. Yeh, T.-E. Nee, J.-I. Chyi, T. M. Hsu, and C. C. Huang, Appl. Phys. Lett. **76**, 1567 (2000).
[38] L. F. Lester, A. Stintz, H. Li, C. Newell, E. A. Pease, B. A. Fuchs, and K. J. Malloy, IEEE Photonics Technol. Lett. **11**, 931 (1999).
[39] G. T. Liu, A. Stintz, H. Li, K. J. Malloy, and L. F. Lester, Electron. Lett. **35**, 1163 (1999).
[40] Xiaodong Huang, A. Stintz, C. P. Hains, G. T. Liu, Julian Cheng, and K. J. Malloy, IEEE Photonics Technol. Lett. **12**, 227 (2000).
[41] I. L. Krestnikov, A. V. Sakharov, N. N. Ledentsov, I. P. Soshnikov, Yu. G. Musikhin, A. R. Kovsh, V. M. Ustinov, I. V. Kochnev, P. S. Kop'ev, Zh. I. Alferov, and D. Bimberg, in *Proceedings of the 6th International Symposium on Nanostructures: Physics and Technology*, St. Petersburg, Ioffe University, St. Petersburg, 1998), p. 257.
[42] A. F. Tsatsul'nikov, N. A. Bedarev, A. R. Kovsh, P. S. Kop'ev, N. A. Maleev, Yu. G. Musikhin, M. V. Maximov, V. M. Ustinov, B. V. Volovik, A. E. Zhukov, N. N. Ledentsov, and D. Bimberg, in *Proceedings of the 26th International Symposium on Compound Semiconductors* (IOP, Bristol, 2000), Berlin, Germany.
[43] M. Arzberger, U. Kasberger, G. Bohm, and G. Abstreiter, Appl. Phys. Lett. **75**, 3968 (1999).
[44] R. Heitz, M. Veit, N. N. Ledentsov, A. Hoffmann, D. Bimberg, V. M. Ustinov, P. S. Kop'ev, and Zh. I. Alferov, Phys. Rev. B **56**, 10 435 (1997).
[45] G. S. Solomon, J. A. Trezza, A. F. Marshall, and J. S. Harris, Phys. Rev. Lett. **76**, 952 (1996).
[46] R. Heitz, I. Mukhametzhanov, P. Chen, and A. Madhukar, Phys. Rev. B **58**, R10 151 (1998).
[47] N. N. Ledentsov, M. V. Maximov, D. Bimberg, T. Maka, C. M. Sotomayor Torres, I. V. Kochnev, I. L. Krestnikov, V. M. Lantratov, N. A. Cherkashin, Yu. M. Musikhin, and Zh. I. Alferov, Semicond. Sci. Technol. **15**, 604 (2000).
[48] M. M. Sobolev, I. V. Kochnev, V. M. Lantratov, N. A. Bert, N. A. Cherkashin, N. N. Ledentsov, D. A. Bedarev, Fiz. Tekh. Poluprovodn. **34**, 200 (2000) [Semiconductors **34**, 195 (2000)].
[49] Kohki Mukai, Yoshiaka Nakata, Koji Otsubo, Mitsuru Sugawara, Naoki Yokoyama, and Hiroshima Ishikawa, IEE J. Quantum Electron. **36**, 472 (2000).
[50] M. V. Maximov, Yu. M. Shernyakov, I. N. Kaiander, D. A. Bedarev, E. Yu. Kondrat'eva, P. S. Kop'ev, A. R. Kovsh, N. A. Maleev, S. S. Mikhrin, A. F. Tsatsul'nikov, V. M. Ustinov, B. V. Volovik, A. E. Zhukov, Zh. I. Alferov, N. N. Ledentsov, and D. Bimberg, Electron. Lett. **35**, 2038 (1999).
[51] Z. Zou, O. B. Shchekin, G. Park, D. L. Huffaker, and D. G. Deppe, IEEE Photonics Technol. Lett. **10**, 1673 (1998).
[52] G. Park, O. B. Shchekin, S. Csutak, and D. G. Deppe, Appl. Phys. Lett. **75**, 3267 (1999).
[53] D. G. Deppe, D. L. Huffaker, S. Csutak, Z. Zou, G. Park, and O. B. Shchekin, IEEE J. Quantum Electron. **35**, 1238 (1999).
[54] S. Seki, H. Oohasi, H. Sugiura, T. Hirono, and K. Yokoyama, J. Appl. Phys. **79**, 2192 (1996).
[55] B. B. Elenkrig, S. Smetona, J. G. Simmons, T. Makino, and J. D. Evans, J. Appl. Phys. **85**, 2367 (1999).
[56] N. N. Ledentsov, D. Bimberg, V. M. Ustinov, J. A. Lott, and Zh. I. Alferov, Memoirs of the Institute of Scientific and Industrial Research, Osaka University **57**, 80 (2000).